

NASA TECHNICAL NOTE



NASA TN D-3072

C-1

NASA TN D-3072

RECEIVED
AFWL (WIL) 2
WRIGHT-PATTERSON AFB, OH

0130070



EXPERIMENTAL PROFILES OF
VELOCITY COMPONENTS AND
RADIAL PRESSURE DISTRIBUTIONS
IN A VORTEX CONTAINED IN
A SHORT CYLINDRICAL CHAMBER

by Joseph M. Savino and Edward G. Keshock

*Lewis Research Center
Cleveland, Ohio*





EXPERIMENTAL PROFILES OF VELOCITY COMPONENTS AND RADIAL
PRESSURE DISTRIBUTIONS IN A VORTEX CONTAINED
IN A SHORT CYLINDRICAL CHAMBER

By Joseph M. Savino and Edward G. Keshock

Lewis Research Center
Cleveland, Ohio

NATIONAL AERONAUTICS AND SPACE ADMINISTRATION

For sale by the Clearinghouse for Federal Scientific and Technical Information
Springfield, Virginia 22151 - Price \$2.00

EXPERIMENTAL PROFILES OF VELOCITY COMPONENTS AND RADIAL PRESSURE DISTRIBUTIONS IN A VORTEX CONTAINED IN A SHORT CYLINDRICAL CHAMBER*

by Joseph M. Savino and Edward G. Keshock**

Lewis Research Center

SUMMARY

An air vortex was generated in a flat cylindrical chamber formed by two 11.72 inch diameter disks that were spaced 1.25 inches apart by 48 vanes equally spaced around the circumference. The vanes were aligned tangentially so that a high swirl was imparted to the air as it entered the chamber. The swirling air was discharged from the chamber through a 2-inch-diameter tube at the center of one disk.

A pitot-yaw probe that sensed both the magnitude and direction of the local velocity vectors was employed to measure the profiles of the radial and tangential velocity components at seven radial stations. A special pitot tube was used to measure the air velocity as it issued from one of the typical vane injection ports. Static pressures were also measured at the same stations.

The resulting profile measurements showed that all the radial inflow occurred in the regions adjacent to the disk surfaces. The axial profiles of the radial velocity component contained two spikes with the maximum occurring at the disk surfaces. The spikes increased in magnitude with decreasing radius. In the midchannel region away from the disk surfaces the radial velocities were small and outward. The tangential velocity profiles were approximately uniform with a slight depression in the center of some. The tangential velocity of the air increased as it moved radially inward.

The frequently employed model, whereby the tangential velocities inside a vortex are predicted from the measured radial pressure distribution, was checked using both the measured static pressures and tangential velocity data. The pressure distribution that was calculated from a balance of the pressure and centrifugal forces using the measured tangential velocities agreed well with the measured static pressure distribution.

From these results and those of investigators cited it was concluded that the tangential-to-radial velocity ratio of the fluid as it is injected into the chamber alone determines what fraction of the total mass flow will be forced to flow inwardly through the end wall boundary layers.

* Presented in an abridged version at Third Fluid Amplification Symposium sponsored by the U.S. Army Materiel Command, Washington, D.C., October 26-28, 1965.

** Presently attending Oklahoma State University, Stillwater, Oklahoma.



INTRODUCTION

Around 1957 and 1958 a rocket engine was conceived whereby a gaseous or solid particulate nuclear fuel was to be contained in a cylindrical chamber by a centrifugal force field. This force field was to be generated by the propellant (hydrogen, e.g.) as it was injected uniformly through the cylinder wall with a high ratio of tangential to radial velocity. Ideally a vortex field would be created as the propellant moved radially inward through the suspended cloud of nuclear fuel toward the central region of the chamber. There the heated propellant would turn and move axially out of the rocket nozzle at the center of one wall. Because of the large density difference between the propellant and the nuclear fuel, the cloud of fuel was to be maintained in a circular orbit by balancing the centrifugal force on the fuel by a radial drag force exerted by the propellant as it diffused through the fuel. Thus, it was hoped that a nearly ideal vortex with negligible end-wall effects could be produced in a cylindrical chamber by injecting the gaseous propellant uniformly everywhere through the cylinder wall with a high ratio of tangential to radial velocity.

A wide-spread interest in the cavity reactor concept developed. Because the nature of confined vortex motions in the presence of end walls was not well understood, many studies, analytical and experimental, were undertaken by various investigators. This study was among them and the results are reported herein.

Preliminary visual experiments were conducted in an attempt to suspend fine particles of various sizes in a vortex of air inside right circular cylinders having length-to-diameter ratios of about one. These studies revealed the presence of some axial motion that always caused the particles to cluster in the corner formed by the cylinder surface and the end wall containing the exit. The fine particles could be seen leaving in a region very close to the end wall while the large particles remained indefinitely. This suggested that a high radial in flow existed in the end-wall boundary layer. From these observations it was obvious that the nature of a confined turbulent vortex could only be determined by direct detailed measurement of the velocity components profiles and the radial pressure distributions. Such a program was undertaken. To prevent the existence of sizeable axial velocity components, an air vortex inside a short cylindrical chamber ($L/D \ll 1$) with planar end walls was chosen for this study.

No literature was available that reported what the influence of the end walls would be in such a vortex. Some results pertaining to the geometry of interest were reported by Kelsall in reference 1, in which he made measurements of the radial, tangential, and axial velocity components inside a hydrocyclone separator. Kelsall's experiments revealed the existence of large secondary motions with most of the mass movement occurring close to all walls where the centrifugal force was lowest. Interestingly enough, the loci of constant tangential velocities were concentric cylinders everywhere except very

close to the walls. Because the geometry and injection conditions of Kelsall's apparatus were considerably different from that of the cavity reactor chamber being considered, his results were not directly applicable. However, they did indicate the importance of stationary surfaces on the motion of confined vortices.

Since the time this work was initiated, many studies, both analytical and experimental, have been conducted into the fluid dynamical characteristics of vortex-type motions. Williamson and McCune (ref. 2) and Donaldson (ref. 3) conducted experiments, in the same apparatus, on short cylinders ($0.130 \leq L/D \leq 0.281$). In both references are reported axial traverses of the total pressure only, and radial distributions of the tangential velocity calculated from these measurements. The latter data in reference 2 (and presumably in ref. 3 also) was evaluated by differentiating the measured static wall pressure and equating this radial pressure gradient to the centrifugal force. The total pressure profiles in both references were quite uniform except for a slight depression in the region far from the end walls.

Ragsdale (refs. 4 and 5) made measurements with a pitot tube in a vortex chamber ($L/D = 0.5$) at two radial stations and several axial stations and deduced in reference 5 that the motion was essentially tangential with very little axial variation in the magnitude. Radial distributions of the static pressure were also determined.

Beverloo, et al. (ref. 6) made radial traverses of the total pressures only with a pitot tube at three axial stations and two angular stations downstream from the single injection slot in short vortex chambers for a variety of injection port and outlet sizes and L/D ratios. Their measurements resulted in the radial distributions of the tangential velocities only.

The most revealing experiments on the distribution of velocities inside vortices have been reported by Kendall (ref. 7) and Donaldson and Williamson (ref. 8). Kendall experimented with a vortex that was generated by a rotating porous cylinder that imparted a swirl to the fluid as it passed through the cylinder into the cavity. The chamber was 6 inches in both length and diameter. The end containing the exit was fixed to the porous cylinder and rotated with it, while the other end was fixed.

Kendall used a flattened pitot tube (which is not normally used for direction measurements because it is not sensitive to yaw angles up to at least $\pm 5^\circ$) to traverse the boundary layer on the fixed end wall for both the total pressure and the local fluid direction under the assumption that at a distance far from the wall the radial velocity was zero and the motion was one of pure tangential velocity. These measurements resulted in profiles of the radial and tangential velocity components. The tangential profile was essentially flat with a slight depression outside the boundary layer. The radial component, on the other hand, was a maximum at the closest measuring station to the wall and decreased monotonically to zero outside the boundary layer. Thus Kendall's profiles showed that the stationary end walls alter the vortex motion considerably and produce a flow pattern in

which a sizable inflow occurs in the boundary layer adjacent to stationary end wall.

More recently Donaldson and Williamson (ref. 8) made measurements of the tangential and radial components and the turbulence in a flat cylinder whose inner and outer radii and length were 1.563, 4.484, and 0.75 inches respectively. The fluid (air) was injected through a rotating porous outer cylinder and removed through stationary porous inner cylinder. A sensitive yaw probe consisting of two beveled tubes was first used to map the local flow directions. Then a pitot tube was inserted and oriented with the local streamlines to measure the local velocity magnitude. A hot wire was employed to determine the mean and fluctuating tangential velocities on the center plane between both end walls. Velocity components were determined at eight axial positions at each of three radial stations for various flow rates and turbulence levels. Because of the manner in which the yaw probe was constructed complete traverses from one end wall to the other were not possible. The resulting profiles revealed the radial inflow was a maximum very close to the end walls and a minimum far from the end walls. A reversal of flow outside the end wall boundary layer region was indicated, but it was assumed to be due to measurement difficulties and therefore nonexistent. The tangential profiles were fairly uniform although several did have a slight depression in the center region of the profile. These results showed that the velocity distributions in a short vortex chamber are quite similar to those found in Kelsall's where the length to diameter ratio was unity.

The theoretical work on confined vortex flows have been concerned with the influence exerted by the end wall flow on the main vortex field for both laminar and turbulent conditions. The approach applied is the momentum integral technique where some reasonable form for the velocity profiles in the boundary layer and the wall skin function laws are assumed. Mack (ref. 9) studied the laminar boundary layer on a finite disk in a rotating flow where a variety of radial distribution of tangential velocity in the freestream were specified. He found that a sizable mass flow occurred in the boundary layer. Rott (ref. 10) examined the sensitivity of the mass flow in a turbulent boundary layer to the assumed form of the shear law and noted that the sensitivity was small. The mutual interaction between the main flow and the boundary layer flow were analyzed by Anderson (refs. 11 and 12) and Rosenzweig, Lewellen, and Ross (ref. 13). For strong vortex flow with high swirl the interaction caused the existence of secondary motion with radial outflow motion in the primary flow. Thus, these analytical studies showed that under certain conditions a part, or all, of the net flow into a vortex passes through the end wall boundary layers.

It was the object of this study, to determine (1) detailed experimental profiles of the velocity components and radial pressures of a vortex confined in one particular geometry, a short cylinder with the plane end walls and (2) to determine which factors are responsible for the resulting profiles. A cylindrical chamber 11.72 inches in diameter and 1.250 inches in length ($L/D = 0.107$) was used as the vortex container. Air was injected

tangentially into the chamber through a series of 48 guide vanes all around the periphery and discharged through a 2.000-inch-diameter exhaust tube that was located at the center of one end wall. This chamber was somewhat similar to that used in references 2, 3, and 8. Axial traverses (24 points) were made at seven radial stations ($r = 1.0, 1.5, 2.0, 2.5, 3.0, 3.5,$ and 4.5 in.) with a probe that sensed both the magnitude and direction of a velocity vector at a point. From these traverses were evaluated the profiles of the radial and tangential velocity components, and the streamline pattern. An additional traverse was made with a pitot tube at the injection radius. Static pressures were also measured at the same radial positions and in addition at $r = 5.61$ inches. The results are presented for only one mass flow rate of 0.209 pound mass per second at an absolute pressure of 42 inches of mercury at $r = 5.61$ inches and temperature of 80° F, although data at higher and lower flows yielded similar results. Hence the conditions were essentially for the incompressible regime.

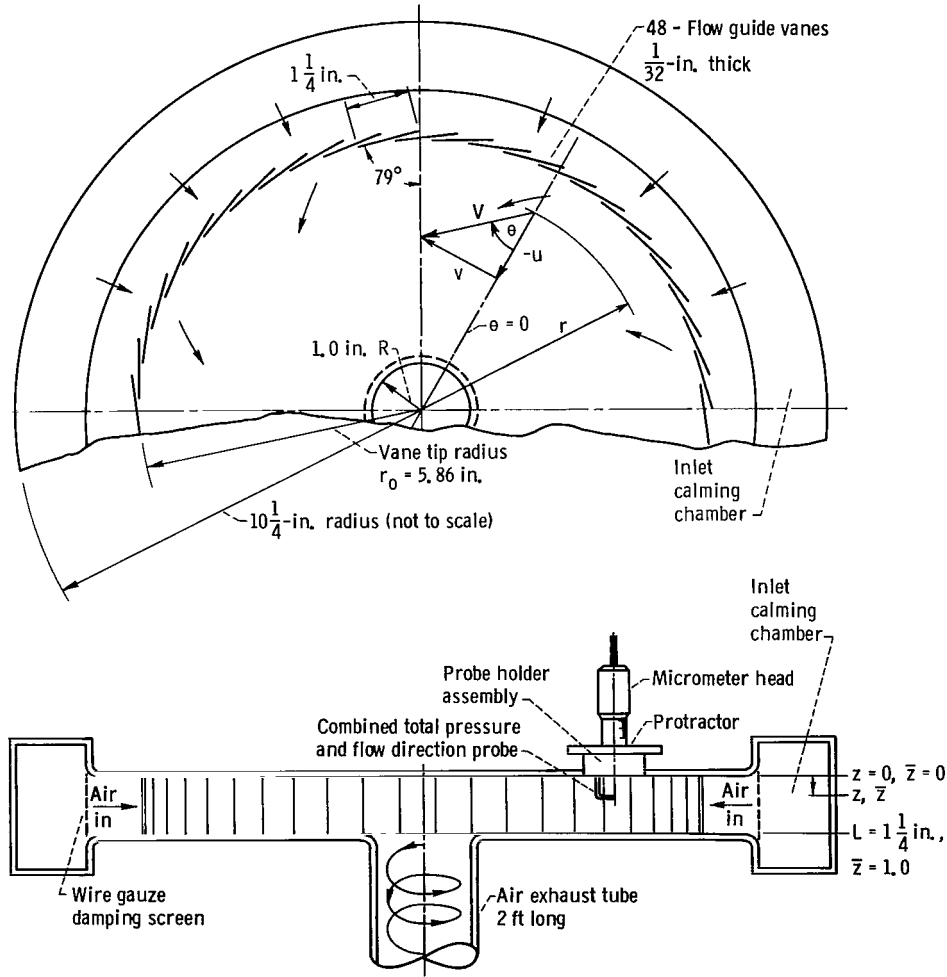


Figure 1. - Schematic arrangement showing essential features of vortex chamber.

APPARATUS

The flat cylindrical vortex chamber is shown schematically in figure 1 (p. 5). The 48 guide vanes imparted a high swirl to the air as it passed inward from the inlet plenum chamber. The wire gauze damping screen aided in producing angular symmetry around the periphery. The end wall opposite the exhaust was fabricated with static wall taps and seven probe ports, each fitted with a removable plug that was flush with the inside surface of the end wall. To make a traverse at a given radial station the plug was removed and the probe holder assembly fastened in its place. Static wall taps 0.010-inch in diameter were drilled at the same radial positions as the probe ports. These taps were located 1 or more inches ahead of the probe station in the angular upstream direction to avoid interference due to the presence of the probe.

It was realized after some preliminary experiments that the velocity component profiles could only be determined with an instrument that was sensitive to the direction as well as the magnitude of any local velocity vector. The conventional pitot tubes that are fabricated from small round tubes are rather insensitive to the yaw and pitch angles up to $\pm 5^\circ$ or more (ref. 14). This is also true of flattened pitot tubes such as the one used in reference 7. Hence, the 3-tube pitot-yaw probe shown in figure 2 was finally chosen because it is very sensitive to yaw in the plane of the three tubes but not to pitch. These two characteristics made the probe quite suitable for this experiment where the axial velocity component was expected to be small. The choice was based on the work of Bryer, Walshe, and Garner (ref. 15).

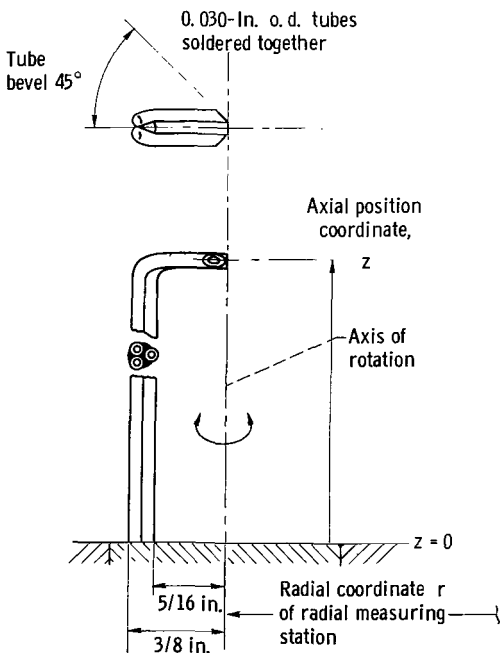


Figure 2. - Three-tube probe for measuring velocity vector magnitude and angular direction.

A second important factor for consideration in the probe selection was its size. Any probe regardless of its size will exert a drag that tends to slow down the vortex. Obviously, the velocities indicated by the probe will differ from those of the undisturbed vortex; the difference increasing with increasing probe size. In addition to slowing down the vortex, the probe size can produce another undesirable effect. If it is used in a region where the motion is very nearly circular, the probe wake will be convected in a circular path so that the probe could be in its own wake. Here again the indicated velocities will differ from those of undisturbed vortex if the wake is too large to be dissipated before it comes back on the probe. Thus, it is seen that while disturbances by the probe cannot altogether be avoided, they can be minimized. To

insure the greatest possible accuracy in this experiment, the probe was made as small as possible consistent with reasonable response times and strength.

The pitot-yaw probe simultaneously measures the magnitude and direction of the impinging fluid stream. The center tube measures the total pressure and the two tubes with beveled ends sense the stream direction. When a tube with a beveled tip is facing up-stream and is aligned with the streamlines of a uniform unidirectional velocity flow field it registers a pressure that is less than the true local total pressure, and this registered pressure is quite sensitive to slight misalignments (ref. 16). Thus, when a pair of beveled tubes are arranged as shown in figure 2 (or without the pitot tube as used in ref. 8) a pressure difference Δp between these tubes is produced, and this pressure difference is quite sensitive to the yaw angle of misalignment ϕ , where ϕ is the angle between the local streamlines and the three tube axes. To measure the local flow direction at a point in a fluid the probe is rotated about its tip as indicated in figure 2, by a suitable mechanism, until the Δp of the yaws tube is zero. Then the angle between the tube axes and a previously established reference angle is measured. The reference angle was chosen to be zero when the probe was aligned with a radial line and directed toward the vortex center.

For these experiments a special holder was made for the three-tube probe. With it

the probe could be positioned axially and rotated into any angular orientation while the tip was always at the same radius. To establish the reference angle the entire assembly was aligned in a 4-inch-diameter unidirectional airstream of uniform velocity. The airstream was produced by a special jet tunnel that was specifically designed for calibrating and aligning probes.

A special pitot tube was made to determine the distribution of the velocity magnitude of the air leaving the injection vanes. No provisions were made to measure the angle of injection with this probe. The probe is shown in figure 3 along with the measured profiles. The total pressure was measured relative to a static wall tap at $r = 5.61$ inches. The true static pressure at the vane outlet was

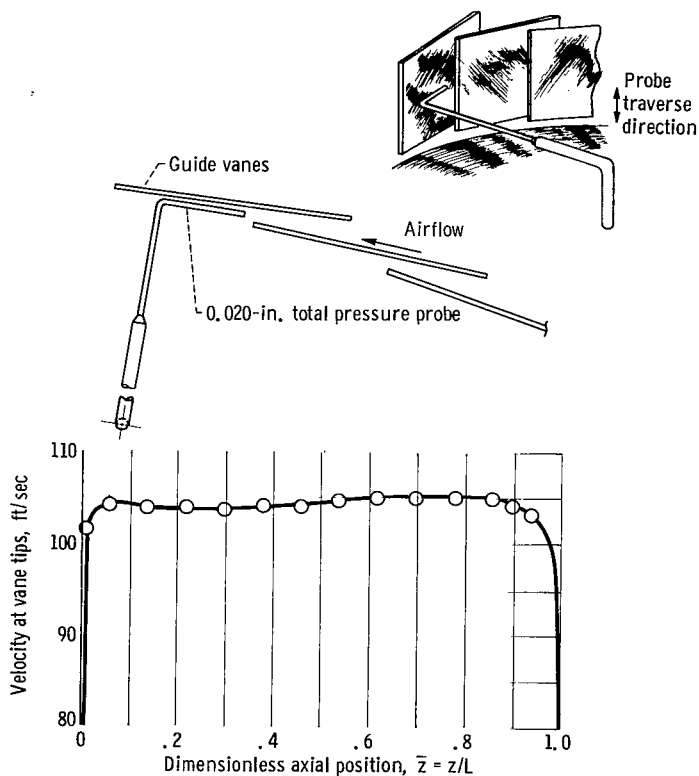


Figure 3. - Velocity profile at guide vane with measuring technique illustrated. Dimensionless radial coordinate, $\bar{r} = 1.0$; mass flow rate = 0.206 lb/sec.

determined by extrapolating the radial static pressure data from $r = 5.61$ to $r \approx 5.9$ inches.

The mass rate of flow through the test section was measured with a calibrated orifice plate that was accurate to within 1/2 percent.

The radial static pressures were measured relative to each other on a group of water manometers the legs of which were all connected to a common well at the lower end. The pressure sensed at the outermost radius, $r = 5.61$ inches, was measured relative to atmosphere on a mercury "U-type" manometer. Water "U-type" manometers were used to measure the difference between (1) the total pressure sensed by the center tube of the pitot-yaw probe and the local static wall pressure at the same radius, (2) the pressures sensed by the beveled yaw tubes of the pitot-yaw probe, (3) the orifice plate pressure difference, and (4) the total pressure of the probe at the vane tips and the wall tap at $r = 5.61$ inches.

The accuracy of the final results depends on the accuracy of the instruments used. All manometers were easily readable to within 0.05 inch. The flow rate was maintained steady within $\pm 1/2$ inch of water out of an overall Δp of 50 inches. The protractor was equipped with a vernier that was readable to 5 minutes and the zero reference was established to within 5 minutes. The micrometer head had a least count of 0.001 inch.

TEST PROCEDURE

To make a typical run, the probe holder was installed in a port at a radius where an axial traverse was desired. The flow of air was started and increased until the desired rate was reached. About 15 minutes were allowed for all manometers to achieve steady-state values. A typical traverse was started with the probe tip completely withdrawn from the flow and touching the wall on which the probe is mounted. The probe was rotated until the pressure difference between the two beveled tubes was zero. The angle was recorded along with the difference between the total pressure sensed by the center tube and the static pressure sensed by the wall tap ahead of it. Then the probe was moved out into the fluid stream to a new position and the procedure was repeated. This was done repeatedly until a complete traverse from one wall to the other was made.

Radial distributions of the static pressures were made both when the probe extended all the way across the channel and when it was completely withdrawn. This was done to note whether the probe exerted any appreciable drag on the vortex.

RESULTS

Velocity Profiles

The velocity traverse made at a typical vane injection slot is shown in figure 3. Velocity directions could not be made with this probe; therefore the plot is only of the velocity magnitude. Figure 3 shows that velocity magnitude was quite uniformly distributed. Because the air was injected through their rectangular slots formed by the flat vanes, it

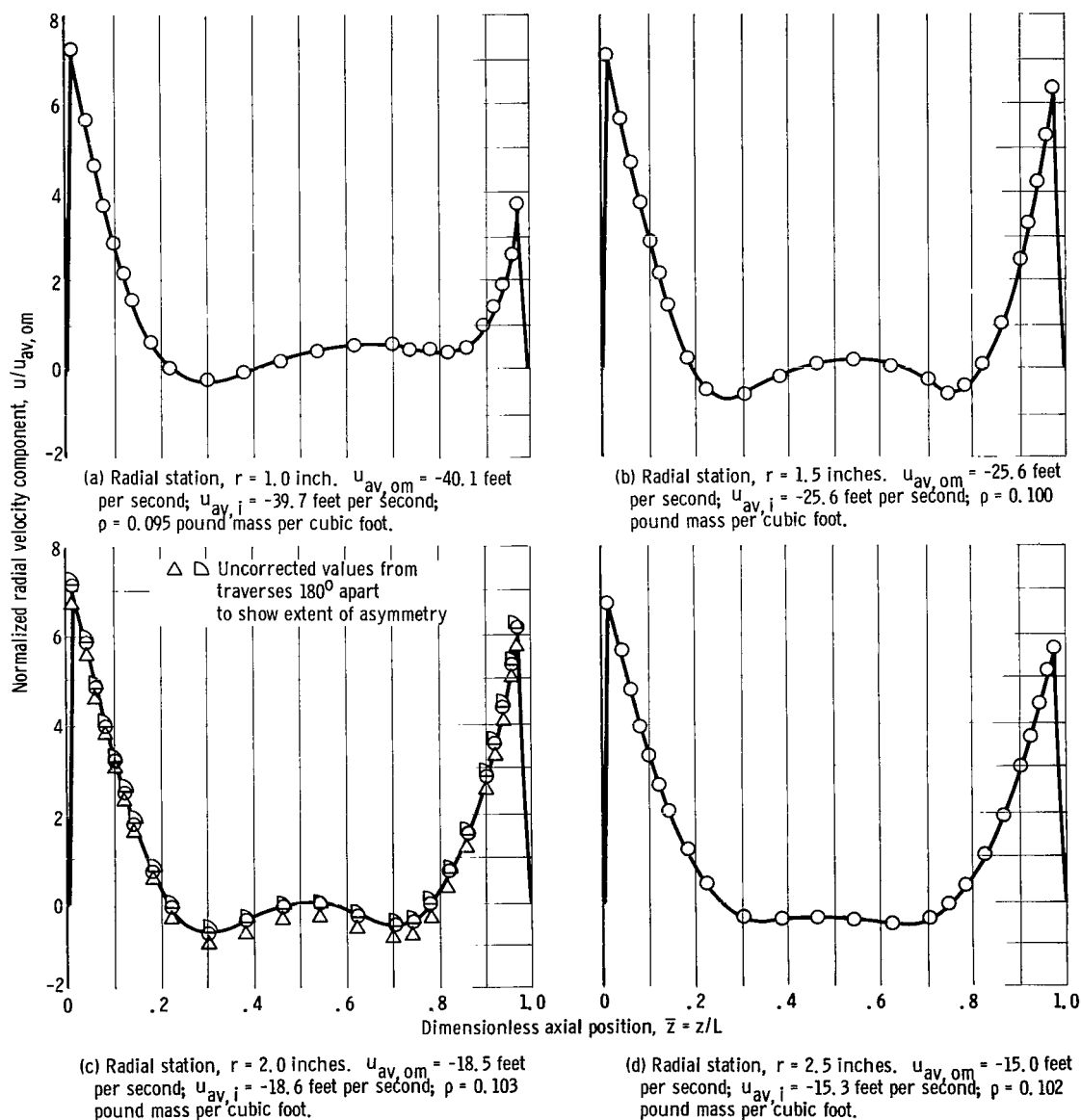


Figure 4. - Dimensionless radial velocity distributions at various radial positions (corrected for asymmetry).

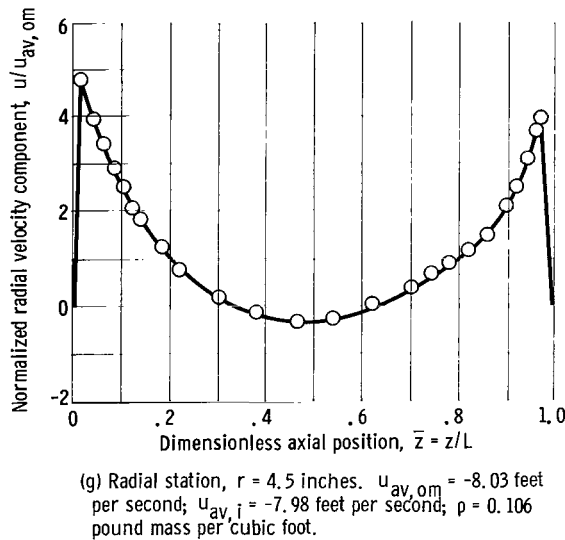
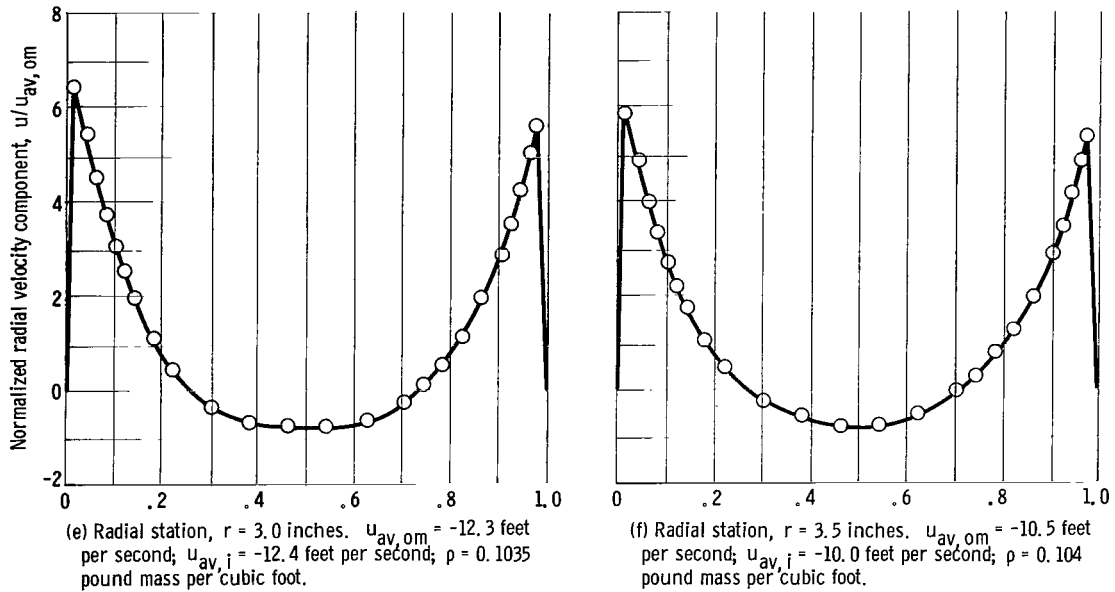


Figure 4. - Concluded.

is believed that uniform injection was also achieved for both the radial and tangential velocities.

The traverse made with the pitot-yaw probe yielded the magnitude V and direction θ' of the local velocity vector. The local radial and tangential velocity components were calculated from relations $u' = V \cos \theta'$ and $v' = V \sin \theta'$. The corrected profiles of the nondimensional radial velocities $u/u_{av,om}$ are given in figure 4, and the dimensional tangential velocities v in figure 5. All the data are also given in greater detail in table I. The streamline pattern depicted in figure 6 (p. 12) was calculated from the definition $\psi(z) = \int_0^z u r dz$ and normalized by the average value $\psi = L r u_{av,om}$. The axial

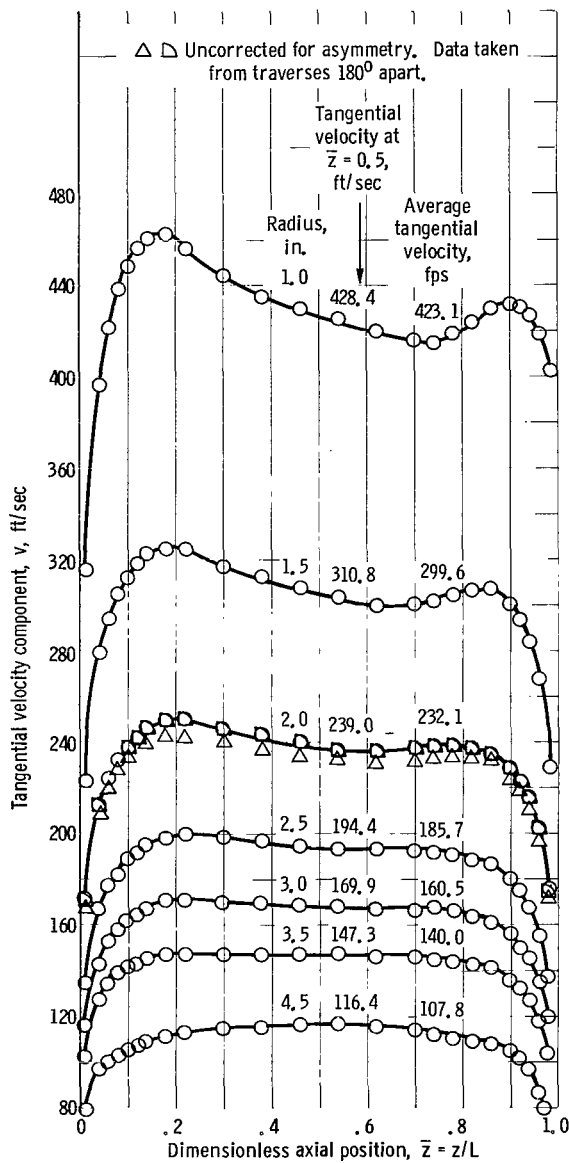


Figure 5. - Dimensional tangential velocity distributions at various radial positions (corrected for asymmetry).

components w were quite small in comparison to the other component over the region where measurements were made. These were calculated from the relation $w = -\frac{1}{r} \frac{\partial}{\partial r} \psi(z)$, but are not shown here. The axial components are probably comparable to u_0 near the vane where the incoming fluid is diverted toward the end walls as indicated by the dotted streamlines.

Figures 3 to 5 reveal several prominent features. The first is the abrupt change in the profile of the radial velocity from a uniform distribution shown in figure 3 (p. 7) to that of figure 4(g). Secondly, figure 4 clearly shows that all of the incoming fluid moves along the end wall toward the exhaust region with the maximum radial velocity occurring very close to the wall. The radial velocities adjacent to the wall are increasing quite rapidly with decreasing radius while away from the walls the radial velocities are small and outward (positive) in direction. The nondimensionalization of u values by the average value $u_{av,om}$ in figure 4 obscures these facts on the one hand, but reveals a similarity of the profile in the boundary layer region on the other. The third feature is that the tangential velocities increase with decreasing radius and that the profiles develop a depression in them. These profiles show the same general features that were independently found in the experiments

by Kendall (ref. 7) and Donaldson and Williamson (ref. 8). One significant difference between profiles of references 7 and 8 and those reported here is the presence of the radial outflow in the mainstream. It is quite possible that the outflow questioned in reference 8 was actually present.

The velocity profiles are caused by several factors: the high swirl ($v_0/u_0 \approx 15$) imparted to the fluid, the no slip condition ($u = v = w = 0$ at $\bar{z} = 0, 1.0$) on the end walls, and the interaction of the high radial inflow with the tangential velocity components. The role of the injection ratio v_0/u_0 is best appreciated by considering the work of Donaldson

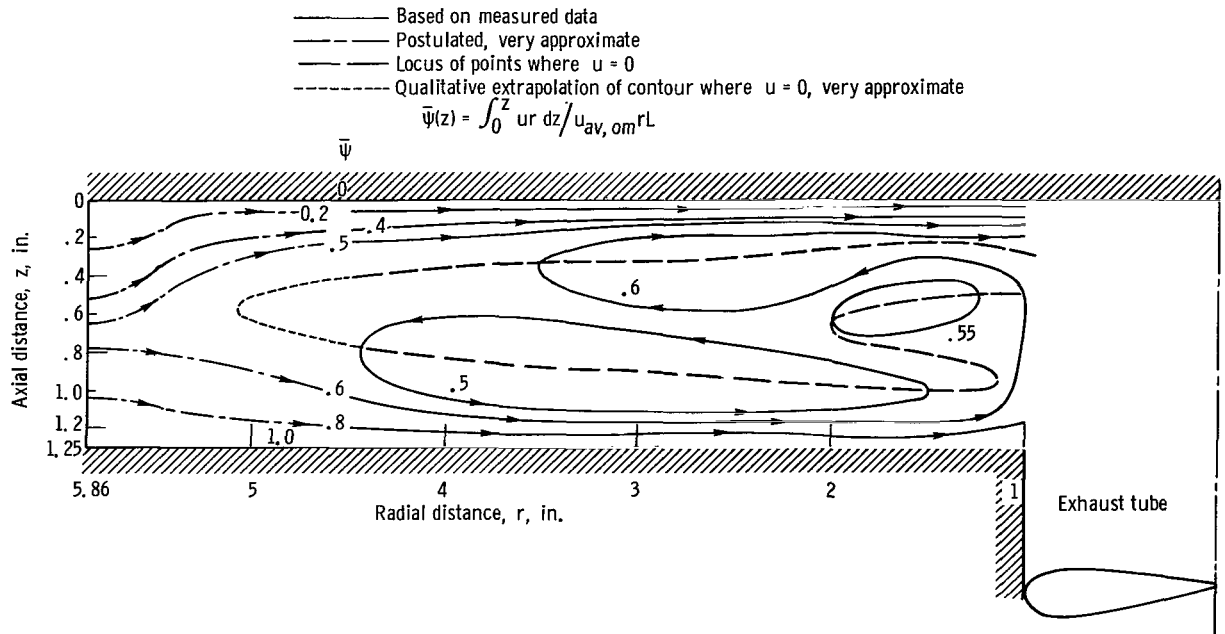


Figure 6. - Pattern of dimensionless streamlines.

and Snedeker (ref. 17) where the influence of variable v_o/u_o ratios was investigated. They experimented with vortex motion inside a rotating porous cylinder, $0 \leq L/D \leq 5$, that was closed at one end by a stationary end wall and open at the other. For $0 < v_o/u_o \lesssim 1.5$, the radial inflow extended to the center and the tangential velocities were distributed approximately like those of an inviscid vortex. As v_o/u_o was increased, $v_o/u_o > 1.5$, the fluid was unable to penetrate the centrifugal field as far, and it turned to move axially out of the chamber at larger radii. Finally, at $v_o/u_o \geq 12$ the fluid turned sharply from radial to axial motion immediately upon entering the vortex chamber, and the tangential motion approached solid body rotation. From these findings it is apparent in the present vortex, where $v_o/u_o \approx 15$, that the air entering the chamber was quickly diverted axially solely because the centrifugal force imparted to the air was considerably higher than its inward momentum. The diverted air entered narrow boundary regions $\Delta z > 0.2$ adjacent to the end walls where it could move radially inward more easily because of the reduced centrifugal force field and increased radial momentum in those regions. The reduced centrifugal field was produced by the no-slip condition on the end walls, and the inward momentum was increased because the effective flow area was reduced and the local inward velocity increased. However, instead of the vortex motion approaching solid-body rotation such as was found in reference 17 for $v_o/u_o > 10$, the tangential velocities approached those of an inviscid vortex. The reason is the fact that some radial inward flow was forced to exist in the present apparatus because two end walls were present whereas such was not the case in reference 17. It is shown in references 17 and 18 that solid-body motion results when no radial velocities exist, and that the

presence of a negative radial velocity in viscous and turbulent vortices interact with the tangential motion causing the motion to depart from solid body rotation and tend toward the inviscid vortex where $v \sim 1/r$ as $-u$ becomes larger in magnitude. In other words, the negative radial velocities tend to preserve angular momentum with complete preservation almost being achieved in the experiment reported here at $\bar{z} = 0.063$ and $\bar{z} = 0.943$. The high centrifugal force field of the boundary regions is then transmitted by tangential turbulent shear to the region away from the boundaries. There a small radial outflow is induced that tends to decrease the angular momentum and cause the depression in the tangential velocity profiles (fig. 5).

The existence of a higher radial mass flow along the end wall opposite the one containing the exhaust port was somewhat unexpected at first glance. A plausible explanation for this situation is the fact that the greatest drag on the vortex by the probe occurred when making the traverses on the end wall with the exhaust port. On the other hand, two other factors that influence the vortex motion could be the cause. They are the radius and length of the exhaust tube. Some unpublished data and observations were recorded on the present vortex chamber when the radius and length of the exhaust tube were varied. The radial pressure distributions inside the exhaust radius were significantly affected by the geometry of the exhaust tube.

Static Pressure Distributions

The measured static pressures are presented in normalized form in figure 7 (p. 14) and in both dimensional and normalized form in table II. The tangential velocity at the vane tips v_0 appearing in the normalization factor ρv_0^2 was extrapolated from the measured values as will be explained.

Also presented for comparison are two curves that were calculated from a simple, frequently used, model with the aid of the measured tangential profiles. It has been common practice in the study of cyclone separators and other vortex devices to evaluate the radial distribution of the tangential velocities from the measured radial distribution of the static pressure under the basic assumption that the radial pressure gradient is produced by the centrifugal force of the fluid. The validity of this assumption can be checked for the present application because both tangential velocities and static pressures were measured.

If in the radial momentum equation for incompressible turbulent fluid motion

$$\rho \left(u \frac{\partial u}{\partial r} + w \frac{\partial u}{\partial z} - \frac{v^2}{r} \right) = - \frac{\partial p_s}{\partial r} + \left(\begin{array}{c} \text{Turbulent} \\ \text{shear} \\ \text{terms} \end{array} \right) \quad (1)$$

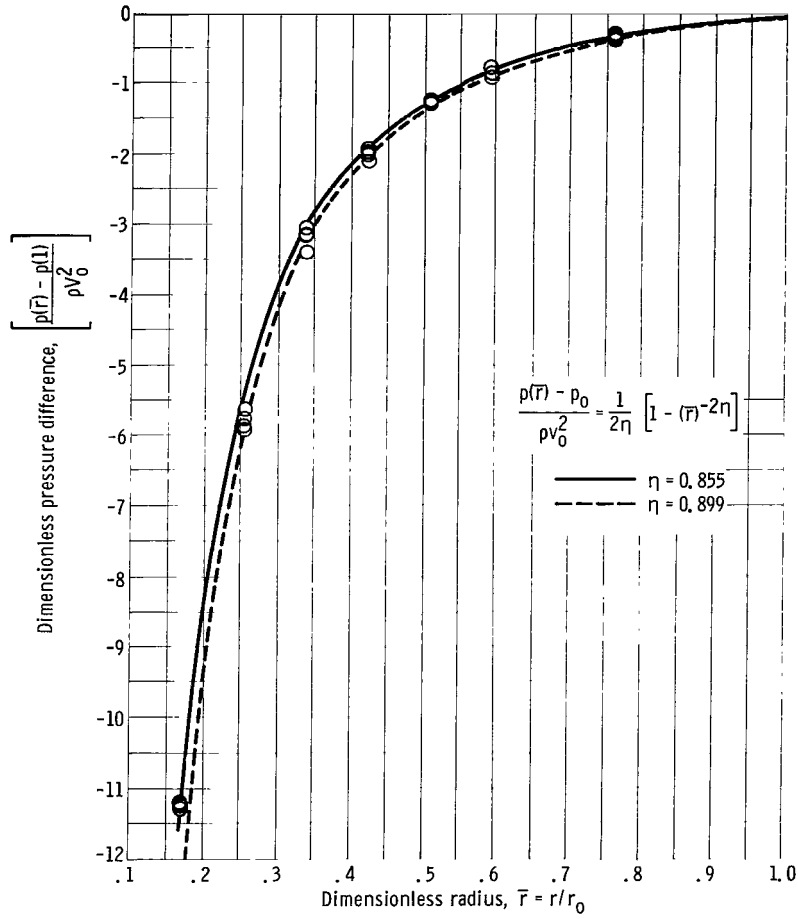


Figure 7. - Comparison of experimentally and analytically determined radial distribution of static pressure.

and the following conditions are met

$$u \frac{\partial u}{\partial z} \ll \frac{v^2}{r} \quad (2a)$$

and

$$w \frac{\partial u}{\partial z} \ll \frac{v^2}{r} \quad (2b)$$

$$\text{turbulent shear terms} \ll \frac{\partial p_s}{\partial r} \quad (2c)$$

then the equation reduces to

$$\rho \frac{v^2}{r} = \frac{dp_s}{dr} \quad (3)$$

The tangential and radial velocity profiles in figures 4 and 5 show that in the midchannel region away from the end walls, the conditions (2a) and (2b) are met because $\partial u/\partial z \approx 0$, $w \approx 0$, and u and $\partial u/\partial r$ are both small; condition (2c) is assumed to hold because the gradients of u and v in the z -direction are small. As is frequently done, let

$$\frac{v}{v_o} = \left(\frac{r}{r_o}\right)^{-n} \quad (4)$$

where n is an experimentally determined exponent. For an inviscid vortex, the equation of motion for the tangential velocity component yields the well known distribution $v \sim 1/r$; that is $n = 1$. When equation (4) is substituted into equation (3) and then equation (3) is integrated, the result is

$$\frac{p_s(\bar{r}) - p_{s,o}(\bar{r} = 1)}{\rho v_o^2} = \frac{1}{2n} \left[1 - (\bar{r})^{-2n} \right] \quad (5)$$

Before equation (5) can be applied a value for n must be chosen from the experimental tangential profile data, and it must fit reasonably well with equation (4). Two choices suggest themselves, one for the v at midchannel ($\bar{z} = 0.5$) where the conditions (2a, b, and c) are satisfied, and the other for the integrated average tangential velocity v_{av} . The best fit through each allowed the data to be extrapolated to $\bar{r} = 1.0$ to give $v_o(\bar{r} = 1, \bar{z} = 0.5)$ and $v_{av,o}$ and the exponent n . The resulting curve fits are

$$\frac{v(\bar{r}, \bar{z} = 0.5)}{v_o(\bar{r} = 1, \bar{z} = 0.5)} = \left(\frac{r}{r_o}\right)^{-0.855} \quad (6)$$

and

$$\frac{v_{av}(\bar{r})}{v_{av,o}} = \left(\frac{r}{r_o}\right)^{-0.899} \quad (7)$$

where $v_o(\bar{r} = 1, \bar{z} = 0.5) = 94.1$ and $v_{av,o} = 86.7$ feet per second. Equations (6) and (7) and the data from which they were derived are given in figure 8 (p. 16). The agreement

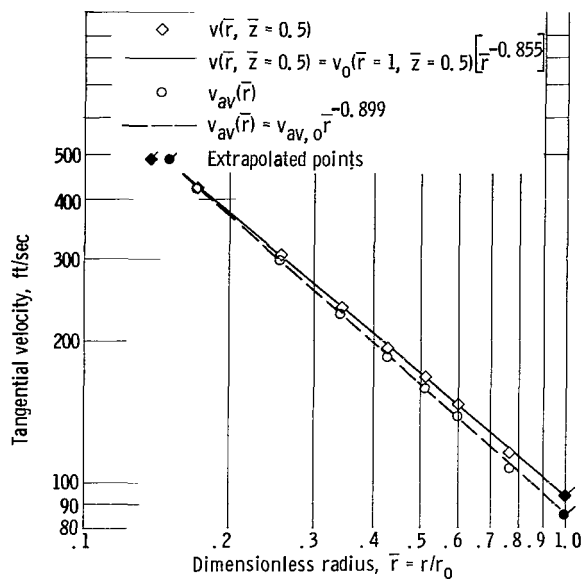


Figure 8. - Radial dependence of experimentally tangent velocities and best-fit curves through data.

between equations (5) for both equations (6) and (7) and the experiment pressures in figure 7 is seen to be very good. The maximum deviation of about 13 percent occurred at $r/r_0 = 0.171$ where the pressure gradients were greatest.

An attempt was made to check equation (3) by differentiating the experimental pressure distribution as was done by Williamson and McCune (ref. 2), but it was not as successful as the preceding approach because of the inherent inaccuracies in differentiating experimental data.

The agreement achieved herein between experimental data and the model verifies the usual assumption that in the body of fluid away from the end walls, the radial pressure

gradient is balanced largely by the centrifugal force. Also the average v_{av} at any r is approximately equal to the value away from the end walls.

Accuracy of Results

The accuracy of the measurements was examined carefully. The static wall pressure data were valid because the wall taps were small (0.010-in. diam), and they were carefully made with square edges free of burrs. The reproducibility of the static pressure data is evidenced in figure 7 and table II where these data were recorded after each velocity traverse.

There was no doubt about the accuracy of the pitot (center) tube of the probe because of its insensitivity to yaw and its long established reliability for velocity measurements in various shear flows. The velocity head readings were repeatable to within a maximum deviation of 1.3 percent. However, because the beveled yaw tubes were used in a field where there were radial as well as axial gradients of the total pressure, each beveled tube was generally exposed to a slightly different local total pressure, even though the spacing between them was small (0.060 in.). As a result the probe could have been yawed relative to the local streamline, when the Δp between them was zero. For this reason a check was made on the accuracy of the θ measurements.

A check on the flow direction data was made as follows. The probe was first alined with the streamlines (yaw angle $\varphi = 0$) of the unidirectional constant-velocity jet

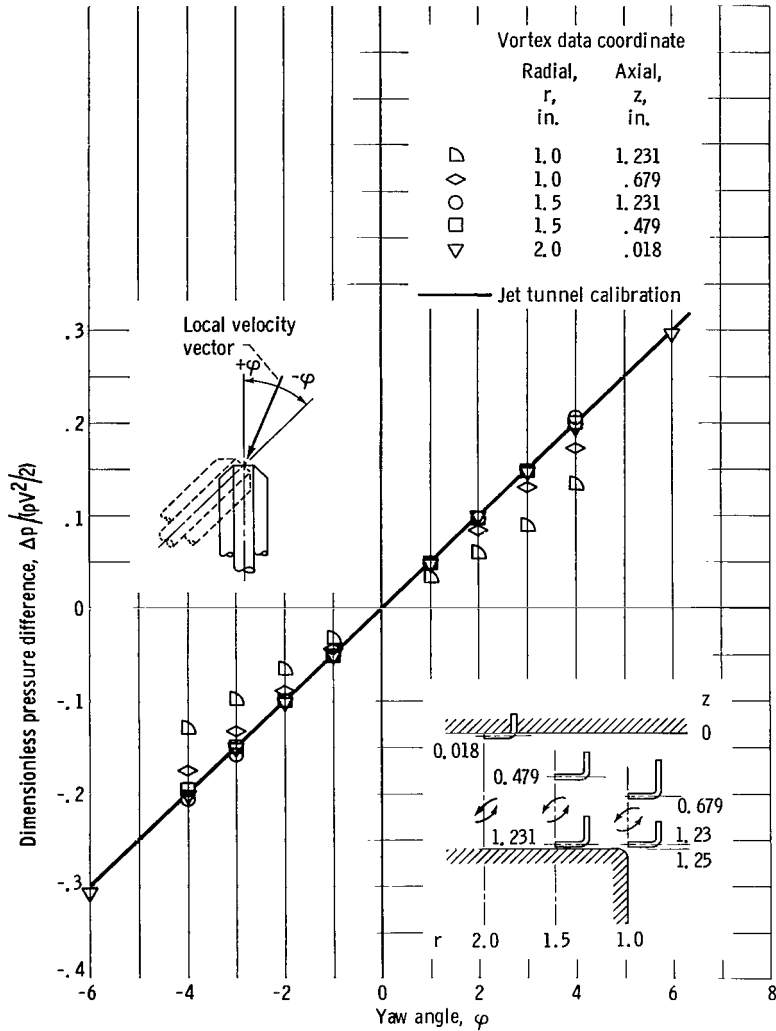


Figure 9. - Dependence of pressure difference between beveled tubes of probe and yaw angle.

mentioned in the section APPARATUS. Then the probe was misaligned over the range of yaw angles $-5^\circ \leq \varphi \leq +5^\circ$ and a curve of the Δp between the yaw tubes against the yaw angle φ was established for the two jet velocities. A similar set of data was recorded at five different positions in the vortex during the final velocity profile measurement runs. The Δp 's of two sets of measurements were normalized by the local velocity pressure $\rho V^2/2$ as registered center tube of the probe, and these are plotted in figure 9. The linear results of figure 9 can be expressed by the relation

$$\frac{\Delta p}{(\rho V^2/2)} = 0.05 \varphi \quad (8)$$

This can be rewritten into the form

$$\varphi = \frac{s}{0.05} \frac{dp_T/dr}{(\rho V^2/2)} \quad (9)$$

where s is the spacing between the centerlines of the beveled tubes and dp_T/dr is the local total pressure gradient.

The possible error φ in the measurement of θ was calculated from equation (9) after having carefully examined all the data and evaluating the local dp_T/dr . The dp_T/dr was, in virtually all cases, small enough that the error φ was within the reading error of the protractor, that is, 5 minutes. Only at the measuring stations closest to the end walls was there any error due to the dp_T/dr , and the error for those few places was less than 0.5° .

Figure 9 deserves additional comment. The nonlinear data at $r = 1.0$ inches reflects the effect of pitch angle between the streamlines and the probe axes. This is not surprising because the air was turning axially into the exhaust tube and the nonlinearity of the data reflects this. The presence of pitch, however, did not effect the accuracy of the θ measurements. The remaining data taken in the vortex is seen to be linear and agrees with the calibration curve. This indicates that the axial velocity component w was negligible relative to u and v at those locations.

A slight azimuthal asymmetry existed in the flow pattern in spite of the precautions to avoid it. Two identical traverses at $r = 2.0$ inches but 180° removed from each other revealed the asymmetry which is shown in figure 4(c) (p. 9) and 5 (p. 11) and table I. These two profiles are similar and differ by a small amount, yet, the integrated mass rates for the uncorrected data of the two traverses at $r = 2.0$ inches (fig. 4(c)) were 0.230 and 0.145 respectively compared to the true value of 0.209 pounds per second as measured by the orifice meter. The large errors in the integrated mass rates occurred primarily because each profile of the radial velocity component in figure 4 has two spikes, and the value of integrated mass rate is quite sensitive to small variations in the profile magnitudes. Although it would have been desirable to have close agreement between the integrated and measured mass flows as a check on the accuracy of the profiles, the shape of the profile made this agreement difficult. Hence, it appears that agreement between the integrated mass flow, and the orifice meter value is not a good method to test the accuracy of the radial velocity profile data. Hence to present a consistent set of graphs the velocity profile data for five out of seven traverses were corrected for the asymmetry by shifting the profile of the measured angles an amount necessary to bring the integrated mass flow to within about 2 percent of the measured profile. The absolute magnitude of the angle correction varied from 0.5 to 1.4 degrees. The correction could have been made on the velocity, or on a combination of angle and velocity. However, since there

appeared to be no factor affecting the choice of correction, the choice was arbitrary. One additional observation merits comment, and that is that the discovery of the asymmetry is additional evidence that the yaw probe was quite sensitive to flow direction.

The presence of the probe exerted a drag on the vortex tending to slow it down. This was evidenced by a shifting of the radial distribution of the static pressure readings as the probe was extended into the stream. The slowdown depended somewhat on the radial location of the probe, the greatest slowdown occurring at the smallest radii, where the velocities were highest, and where the probe was fully extended across the vortex. The maximum shift in the radial pressure distribution amounted to 1 part in 6 of the undisturbed distribution that is shown in figure 7 (p. 14). On the average for most of the data the effect of the drag was considerably less. No attempt was made to correct the velocity profiles for the effects of probe drag because it appeared impossible to do accurately.

An attempt was made to assess the effect of the probe wake by injecting helium into the vortex with a probe-like injection tube and recording Schlieren photos. It appeared that any disturbance created by the probe was dissipated so that the probe wake did not seem to propagate back on itself. The schlieren photos also confirmed that the motion was turbulent everywhere. Hence, it was concluded that the presence of the probe wake was producing a negligible effect on the profiles.

The extrapolated value of v_o and $v_{av,o}$ were 94.1 and 86.7 feet per second as compared with an average of about 104.5 feet per second measured at the vane tip shown in figure 3 (p. 7). This variation was expected because there exists local mixing of the jets as they emerge from the vane injection slots.

CONCLUSIONS

The purpose of this study was to make accurate measurements of the radial and tangential velocities throughout the vortex and of the radial static pressures and to determine the factors that influence the motion. This goal was achieved, and from the results presented herein and those of the investigators cited, the following conclusions are drawn concerning the factors that influence confined vortex motion. In particular, these conclusions apply to cylindrical chambers that have stationary planar end walls with an exhaust hole, much smaller in diameter than the cylinder, in one (or possibly both) of them, and a L/D ratio less than approximately 2.

The amount of swirl (the ratio of tangential to radial velocities) imparted to the fluid as it is injected into the chamber alone determines what fraction of the total mass flow will be forced to flow inwardly within the end wall boundary layers. When the swirl is low, a tangential-to-radial velocity ratio less than approximately 1 to 2, the radial inflow will have enough inward momentum to penetrate the centrifugal field, and inflow will exist

at all axial and radial positions away from the walls. When the swirl is high as it was in the present work with velocity ratios above roughly 10, the radial inflow is diverted axially; and if two stationary end walls are present, all the fluid leaves the chamber by way of the boundary regions adjacent to these end walls. However, if at least one end of the chamber is wide open, the fluid would discharge immediately out of this end. Because the centrifugal force field near the walls is reduced due to the no-slip condition on the surface, inward radial velocities exist there, and they tend to conserve angular momentum. This accounts for the approximate inviscid-like vortex motion.

The simple model whereby the centrifugal forces are balanced only by the radial pressure is valid in regions far removed from the end walls.

Lewis Research Center,
National Aeronautics and Space Administration,
Cleveland, Ohio, August 10, 1965.

APPENDIX - SYMBOLS

<p>D vortex chamber outer diameter, $2 r_o$</p> <p>L vortex chamber length</p> <p>n exponent appearing in equation (4)</p> <p>p pressure</p> <p>r dimensional radial coordinate</p> <p>\bar{r} dimensionless radial coordinate, r/r_o</p> <p>u radial velocity component</p> <p>V velocity vector magnitude</p> <p>v tangential velocity component</p> <p>w axial velocity component</p> <p>z dimensional axial coordinate</p> <p>\bar{z} dimensionless axial coordinate, z/L</p> <p>θ angle measured from radial line to local velocity vector</p>	<p>ρ fluid density</p> <p>φ yaw angle</p> <p>ψ stream function</p> <p>$\bar{\psi}$ dimensionless stream function</p> <p>Subscripts</p> <p>av average value</p> <p>i integral value</p> <p>o value at outer vortex radius, $r_o = 5.86$ in.</p> <p>om value calculated from orifice meter flow rate</p> <p>s static pressure</p> <p>T designates total pressure</p> <p>' prime denotes the indicated values</p>
--	--

REFERENCES

1. Kelsall, D.F.: A Study of the Motion of Solid Particles in a Hydraulic Cyclone. Trans. Inst. Chem. Engrs., vol. 30, 1952, pp. 87-108.
2. Williamson, G.G.; and McCune, J.E.: A Preliminary Study of the Structure of Turbulent Vortices. Rept. No. 32, Aeron. Res. Assoc. of Princeton, Inc., July 1961.
3. Donaldson, Coleman duP.: The Magneto-hydrodynamic Vortex Power Generator, Basic Principles and Practical Problems. Rept. No. 30, Aeron. Res. Assoc. of Princeton, Inc., Mar. 1961.
4. Savino, Joseph M.; and Ragsdale, Robert G.: Some Temperature and Pressure Measurements in Confined Vortex Fields. J. Heat Transfer (Trans. ASME), ser. C, vol. 83, no. 1, Feb. 1961, pp. 33-38.
5. Ragsdale, Robert G.: Applicability of Mixing Length Theory to a Turbulent Vortex System. NASA TN D-1051, 1961.
6. Beverloo, W.A.; Leniger, H.A.; and Weldring, J.A.G.: Potentialities of the Flat Vortex Hydrosifter. Brit. Chem. Eng. J., vol. 8, no. 10, Oct. 1963, pp. 678-682.
7. Kendall, James M., Jr.: Experimental Study of a Compressible Viscous Vortex. Tech. Rept. No. 32-290, Jet Prop. Lab., C.I.T., June 5, 1962.
8. Donaldson, C. duP.; and Williamson, Guy G.: An Experimental Study of Turbulence in a Driven Vortex. Aeron. Res. Assoc. of Princeton, Rept. No. ARAP TM-64-2, Aeron. Res. Assoc. of Princeton, Inc., July 1964.
9. Mack, Leslie M.: The Laminar Boundary Layer on a Disk of Finite Radius in a Rotating Flow, pt. 1. Tech. Rept. No. 32-224, Jet Prop. Lab., C.I.T., May 20, 1962.
10. Rott, N.: Turbulent Boundary Layer Development on the End Walls of a Vortex Chamber. Rept. No. ATN-62(9202)-1, Aerospace Corp., July 30, 1962.
11. Anderson, Olaf L.: Theoretical Solutions for the Secondary Flow on the End Wall of a Vortex Tube. Rept. No. R-2492-1, United Aircraft Corp., Nov. 1961.
12. Anderson, O.L.: Theoretical Effect of Mach Number and Temperature Gradient on Primary and Secondary Flows in a Jet-Driven Vortex. Rept. No. RTD-TDR-63-1098, United Aircraft Corp., Nov. 1963.
13. Rosenzweig, M.L.; Lewellen, W.S.; and Ross, D.H.: Confined Vortex Flows with Boundary-Layer Interactions. AIAA J., vol. 2, no. 12, Dec. 1964, pp. 2127-2134.

14. Gracey, William; Letko, William; and Russell, Walter R. : Wind-Tunnel Investigation of a Number of Total-Pressure Tubes at High Angles of Attack. Subsonic Speeds. NACA TN 2331, 1951.
15. Bryer, D.W. ; Walshe, D.E. ; and Garner, H.G. : Pressure Probes Selected for Three-Dimensional Flow Measurement. R. & M. No. 3037, British ARC, 1958.
16. Schulze, W.M. ; Ashby, G.C. , Jr. ; and Erwin, J.R. : Several Combination Probes for Surveying Static and Total Pressure and Flow Direction. NACA TN 2830, 1952.
17. Donaldson, C. duP. ; and Snedeker, R.S. : Experimental Investigation of the Structure of Vortices in Simple Cylindrical Vortex Chambers. Rept. No. 47, Aeron. Res. Assoc. of Princeton, Inc. , Dec. 1962.
18. Donaldson, C. duP. : Solutions of the Navier-Stokes Equations for Two and Three-Dimensional Vortices. Ph.D. Thesis, Princeton Univ. , 1957.

TABLE I. - VELOCITY COMPONENTS DATA

(a) Radial station, 1.0 inch. Temperature, 75⁰ F; density, 0.0954 pound mass per square foot; absolute pressure, 38.7 inches of mercury.

Axial coordinate		Velocity vector magnitude V, ft/sec	Velocity vector direction		Radial velocity component ^a			Tangential velocity component ^b	
z, in.	$\bar{z} = z/L$		Observed θ' , deg	Corrected θ , deg	Observed u', ft/sec	Corrected u, ft/sec	Normalized u/u _{av,om}	Observed v', ft/sec	Corrected v, ft/sec
0.018	0.014	427.9	48.00	47.50	-286.34	-289.10	-7.201	318.0	315.5
.054	.043	456.4	60.92	60.42	-221.86	-225.33	-5.612	398.9	396.9
.079	.063	460.3	66.92	66.42	-180.45	-184.14	-4.586	423.4	421.8
.104	.083	463.3	71.92	71.42	-143.80	-147.64	-3.677	440.4	439.1
.129	.103	463.9	76.08	75.58	-111.56	-115.49	-2.877	450.2	449.3
.154	.123	464.8	79.67	79.17	-83.37	-87.36	-2.176	457.3	456.5
.179	.143	464.8	82.67	82.17	-59.32	-63.35	-1.578	461.0	460.5
.229	.183	463.3	87.42	86.92	-20.88	-24.92	-.621	462.8	462.6
.279	.223	456.4	90.33	89.83	2.65	-1.33	-.033	456.4	456.4
.379	.303	444.4	91.92	91.42	14.87	10.99	.274	444.1	444.3
.479	.383	435.2	90.92	90.42	6.97	3.17	.079	435.2	435.2
.579	.463	430.4	89.58	89.08	-3.13	-6.89	-.172	430.4	430.3
.679	.543	426.3	88.67	88.17	-9.92	-13.64	-.340	426.2	426.1
.779	.623	420.9	87.75	87.25	-16.53	-20.19	-.503	420.6	420.4
.879	.703	417.4	87.58	87.08	-17.60	-21.24	-.529	417.0	416.8
.929	.743	416.1	87.83	87.33	-15.73	-19.36	-.482	415.8	415.7
.979	.783	419.7	88.25	87.75	-12.82	-16.48	-.411	419.5	419.3
1.029	.823	424.9	88.58	88.08	-10.51	-14.21	-.354	424.7	424.6
1.079	.863	430.8	87.92	87.42	-15.66	-19.41	-.483	430.5	430.3
1.129	.903	434.0	85.42	84.92	-34.68	-38.45	-.958	432.6	432.3
1.154	.923	434.6	83.17	82.67	-51.71	-55.47	-1.382	431.5	431.1
1.179	.943	434.0	80.33	79.83	-72.88	-76.61	-1.908	427.9	427.2
1.204	.963	432.4	76.58	76.08	-100.33	-104.00	-2.590	420.6	419.7
1.231	.985	430.0	70.33	69.83	-144.71	-148.23	-3.692	404.9	403.6

^aAverage radial velocities, $u_{av,om} = 40.15$ ft/sec, $u'_{av,i} = -36.01$ ft/sec, $u_{av,i} = -39.70$ ft/sec.

^bAverage tangential velocity, $v_{av,i} = 423.1$ ft/sec.

TABLE I. - Continued. VELOCITY COMPONENTS DATA

(b) Radial station: 1.5 inches. Temperature, 78° F; density, 0.100 pound mass per cubic foot; absolute pressure, 40.6 inches of mercury.

Axial coordinate		Velocity vector magnitude V, ft/sec	Velocity vector direction		Radial velocity component ^a			Tangential velocity component ^b	
z, in.	$\bar{z} = z/L$		Observed θ' , deg	Corrected θ , deg	Observed u', ft/sec	Corrected u, ft/sec	Normalized u/u _{av,om}	Observed v', ft/sec	Corrected v, ft/sec
0.018	0.014	288.1	50.25	50.75	-184.20	-182.26	-7.111	221.5	223.1
.054	.043	315.3	61.92	62.42	-148.42	-145.99	-5.696	278.2	279.5
.079	.063	318.2	67.33	67.83	-122.63	-120.06	4.684	293.6	294.7
.104	.083	320.0	71.92	72.42	-99.34	-96.68	-3.772	304.2	305.1
.129	.103	321.1	76.00	76.50	-77.68	-74.96	-2.925	311.6	312.2
.154	.123	323.2	79.52	80.02	-58.80	-56.02	-2.186	317.8	318.3
.179	.143	324.7	82.83	83.33	-40.51	-37.70	-1.471	322.2	322.5
.229	.183	325.0	88.17	88.67	-10.39	-7.56	-.295	324.8	324.9
.279	.223	325.0	91.58	92.08	8.98	11.81	.461	324.9	324.8
.379	.303	317.9	92.08	92.58	11.56	14.33	.559	317.7	317.6
.479	.383	313.2	90.17	90.67	.91	3.65	.142	313.2	313.1
.579	.463	308.0	89.00	89.50	-5.38	-2.69	-.105	308.0	308.0
.679	.543	304.2	88.58	89.08	-7.52	-4.87	-.190	304.1	304.2
.779	.623	300.6	89.33	89.83	-3.50	-.88	-.034	300.6	300.6
.879	.703	301.4	90.50	91.00	2.63	5.26	.205	301.4	301.4
.929	.743	302.8	92.08	92.58	11.01	13.65	.533	302.6	302.5
.979	.783	305.3	91.42	91.92	7.55	10.21	.398	305.2	305.1
1.029	.823	307.8	88.92	89.42	-5.82	-3.13	-.122	307.7	307.7
1.079	.863	308.8	84.50	85.00	-29.60	-26.92	-1.050	307.4	307.7
1.129	.903	307.8	77.50	78.00	-66.61	-63.99	-2.497	300.5	301.0
1.154	.923	306.4	73.42	73.92	-87.45	-84.88	-3.312	293.7	294.4
1.179	.943	304.5	68.67	69.17	-110.76	-108.28	-4.225	283.6	284.6
1.204	.963	300.6	62.67	63.17	-138.02	-135.68	-5.294	267.0	268.2
1.231	.985	281.6	54.08	54.68	-165.18	-163.19	-6.367	228.1	229.5

^a Average radial velocities, $u_{av,om} = -25.6$ ft/sec, $u'_{av,i} = -28.2$ ft/sec, $u_{av,i} = -25.6$ ft/sec.

^b Average tangential velocity, $v_{av,i} = 299.6$ ft/sec.

TABLE I. - Continued. VELOCITY COMPONENTS DATA

(c₁) Radial station: 2.0 inches 180° removed from (c₂). Temperature, 76° F; density, 0.103 pound mass per cubic foot; absolute pressure, 41.70 inches of mercury.

Axial coordinate		Velocity vector magnitude V, ft/sec	Velocity vector direction		Radial velocity component ^a			Tangential velocity component ^b	
z, in.	$\bar{z} = z/L$		Observed θ' , deg	Corrected θ , deg	Observed u', ft/sec	Corrected u, ft/sec	Normalized u/u _{av,om}	Observed v', ft/sec	Corrected v, ft/sec
0.018	0.014	217.1	51.83	52.33	-134.18	-132.68	-7.118	170.7	171.9
.054	.043	238.9	62.33	62.83	-110.92	-109.07	-5.851	211.6	212.5
.079	.063	241.9	67.67	68.17	-91.93	-89.97	-4.827	223.8	224.6
.104	.083	243.9	71.83	72.33	-76.05	-74.03	-3.971	231.8	232.4
.129	.103	245.3	75.50	76.00	-61.41	-59.33	-3.183	237.4	238.0
.154	.123	246.3	78.75	79.25	-48.04	-45.93	-2.464	241.5	241.9
.179	.143	248.6	81.83	82.33	-35.31	-33.16	-1.779	246.0	246.3
.229	.183	249.9	86.58	87.08	-14.89	-12.71	-.682	249.4	249.5
.279	.223	250.2	90.00	90.50	0	2.18	.117	250.2	250.2
.379	.303	246.6	92.58	93.08	11.11	13.26	.711	246.3	246.2
.479	.383	243.9	91.58	92.08	6.74	8.87	.476	243.8	243.8
.579	.463	240.6	90.08	90.58	.35	2.45	.131	240.6	240.6
.679	.543	237.2	89.92	90.42	-.34	1.73	.093	237.2	237.2
.779	.623	237.2	91.00	91.50	4.14	6.21	.333	237.1	237.1
.879	.703	238.5	92.00	92.50	8.32	10.40	.558	238.4	238.3
.929	.743	239.2	91.67	92.17	6.96	9.05	.486	239.1	239.0
.979	.783	239.2	89.92	90.42	-.35	1.74	.093	239.2	239.2
1.029	.823	238.5	86.75	87.25	-13.52	-11.44	-.612	238.2	238.2
1.079	.863	237.2	82.75	83.25	-29.93	-27.88	-1.496	235.3	235.3
1.129	.903	235.5	76.75	77.25	-53.96	-51.96	-2.787	229.2	229.6
1.154	.923	232.7	73.17	73.67	-67.38	-65.43	-3.510	222.7	223.3
1.179	.943	231.3	69.00	69.50	-82.88	-80.99	-4.345	215.9	216.6
1.204	.963	225.9	63.58	64.08	-100.52	-98.75	-5.298	202.3	203.2
1.231	.985	210.3	56.58	57.08	-115.81	-114.27	-6.130	175.5	176.5

^a Average radial velocities, $u_{av,om} = -18.6$ ft/sec, $u'_{av,i} = -20.5$ ft/sec, $u_{av,i} = -18.5$ ft/sec.

^b Average tangential velocity, $v_{av,i} = 232.1$ ft/sec.

TABLE I. - Continued. VELOCITY COMPONENTS DATA

(c₂) Radial station, 2.0 inches. Temperature, 83° F; density, 0.102 pound mass per cubic foot; absolute pressure, 42.0 inches of mercury.

Axial coordinate		Velocity vector magnitude V, ft/sec	Velocity vector direction		Radial velocity component ^a			Tangential velocity component ^b	
z, in.	$\bar{z} = z/L$		Observed θ' , deg	Corrected θ , deg	Observed u', ft/sec	Corrected u, ft/sec	Normalized u/u _{av,om}	Observed v', ft/sec	Corrected v, ft/sec
0.018	0.014	208.7	53.33	51.93	-124.61	-128.67	-6.854	167.4	164.3
.054	.043	232.8	63.67	62.27	-103.26	-108.33	-5.771	208.6	206.0
.079	.063	235.6	68.75	67.35	-85.38	-90.72	-4.833	219.6	217.4
.104	.083	237.3	72.92	71.52	-69.71	-75.23	-4.008	226.8	225.1
.129	.103	239.0	76.58	75.18	-55.46	-61.13	-3.256	232.5	231.1
.154	.123	240.7	80.00	78.60	-41.80	-47.58	-2.535	237.1	236.0
.179	.143	241.4	83.08	81.68	-29.07	-34.92	-1.860	239.7	238.9
.229	.183	243.4	87.92	86.52	-8.85	-14.79	-.789	243.3	243.0
.279	.223	243.4	91.75	90.35	7.43	1.49	.079	243.3	243.4
.379	.303	240.7	94.42	93.02	18.54	12.67	.674	240.0	240.4
.479	.383	237.3	93.33	91.93	13.80	8.00	.426	236.9	237.2
.579	.463	234.2	92.00	90.60	8.17	2.45	.131	234.0	234.2
.679	.543	232.1	91.83	90.43	7.42	1.75	.093	232.0	232.1
.779	.623	231.0	92.92	91.52	11.76	6.12	.326	230.7	230.9
.879	.703	232.4	94.00	92.60	16.21	10.54	.561	231.9	232.2
.929	.743	233.8	93.67	92.27	14.96	9.25	.493	233.4	233.7
.979	.783	233.8	91.92	90.52	7.82	2.11	.112	233.7	233.8
1.029	.823	233.1	88.83	87.43	-4.75	-10.44	.556	233.1	232.9
1.079	.863	232.4	84.58	83.18	-21.94	-27.59	-1.470	231.4	230.8
1.129	.903	228.5	78.33	76.93	-46.21	-51.67	-2.753	223.8	222.6
1.154	.923	226.7	74.67	73.27	-59.95	-65.28	-3.478	218.7	217.1
1.179	.943	223.8	70.33	68.93	-75.33	-80.45	-4.286	210.8	208.9
1.204	.963	217.9	64.58	63.18	-93.52	-98.30	-5.237	196.8	194.5
1.228	.982	201.5	58.25	56.85	-106.03	-110.18	-5.869	171.3	168.7

^aAverage radial velocities, $u_{av,om} = -18.8$ ft/sec, $u'_{av,i} = -13.0$ ft/sec, $u_{av,i} = -18.6$ ft/sec.

^bAverage tangential velocity, $v_{av,i}$ not calculated.

TABLE I. - Continued. VELOCITY COMPONENTS DATA

(d) Radial station, 2.5 inches. Temperature, 81° F; density, 0.102 pound mass per cubic foot; absolute pressure, 41.8 inches of mercury.

Axial coordinate		Velocity vector magnitude V, ft/sec	Velocity vector direction		Radial velocity component ^a			Tangential velocity component ^b	
z, in.	$\bar{z} = z/L$		Observed θ' , deg	Corrected θ , deg	Observed u', ft/sec	Corrected u, ft/sec	Normalized u/u _{av,om}	Observed v', ft/sec	Corrected v, ft/sec
0.018	0.014	167.9	54.33	53.33	-97.87	-100.24	-6.671	136.4	134.6
.054	.043	187.2	64.25	63.25	-81.34	-84.27	-5.608	168.6	167.2
.079	.063	190.7	69.25	68.25	-67.56	-70.66	-4.702	178.3	177.1
.104	.083	190.7	73.25	72.25	-54.96	-58.14	-3.869	182.6	181.6
.129	.103	195.4	76.58	75.58	-45.33	-48.64	-3.237	190.0	189.2
.154	.123	194.9	79.50	78.50	-35.53	-38.87	-2.587	191.7	191.0
.179	.143	197.0	82.25	81.25	-26.57	-29.97	-1.994	195.2	194.7
.229	.183	198.3	86.42	85.42	-12.39	-15.84	-1.054	197.9	197.6
.279	.223	199.9	89.67	88.67	-1.16	-4.65	-0.309	199.9	199.9
.379	.303	198.3	92.75	91.75	9.51	6.06	.403	198.1	198.2
.479	.383	197.0	93.17	92.17	10.89	7.45	.496	196.7	196.9
.579	.463	194.9	93.00	92.00	10.20	6.80	.453	194.7	194.8
.679	.543	194.1	93.17	92.17	10.72	7.34	.488	193.8	194.0
.779	.623	194.1	93.58	92.58	12.13	8.75	.582	193.7	193.9
.879	.703	193.3	93.00	92.00	10.11	6.74	.449	193.0	193.1
.929	.743	192.4	91.67	90.67	5.60	2.24	.149	192.3	192.4
.979	.783	191.6	89.67	88.67	-1.11	-4.46	-.297	191.6	191.5
1.029	.823	189.8	86.50	85.50	-11.59	-14.89	-.991	189.5	189.3
1.079	.863	189.0	82.50	81.50	-24.67	-27.93	-1.859	187.4	186.9
1.129	.903	185.9	77.00	76.00	-41.82	-44.98	-2.993	181.2	180.4
1.154	.923	184.1	73.58	72.58	-52.04	-55.12	-3.668	176.6	175.7
1.179	.943	181.0	69.58	68.58	-63.14	-66.09	-4.398	169.6	168.5
1.204	.963	174.1	64.50	63.50	-74.94	-77.68	-5.170	157.1	155.8
1.225	.980	161.9	59.42	58.42	-82.37	-84.79	-5.643	139.4	137.9

^aAverage radial velocities, $u_{av,om} = -15.0$ ft/sec, $u'_{av,i} = -12.1$ ft/sec, $u_{av,i} = -15.3$ ft/sec.

^bAverage tangential velocity, $v_{av,i} = 185.7$ ft/sec.

TABLE I. - Continued. VELOCITY COMPONENTS DATA

(e) Radial station, 3.0 inches. Temperature, 81° F; density, 0.104 pound mass per cubic foot; absolute pressure, 42.4 inches of mercury.

Axial coordinate		Velocity vector magnitude V, ft/sec	Velocity vector direction		Radial velocity component ^a			Tangential velocity component ^b	
z, in.	$\bar{z} = z/L$		Observed θ' , deg	Corrected θ , deg	Observed u', ft/sec	Corrected u, ft/sec	Normalized u/u _{av,om}	Observed v', ft/sec	Corrected v, ft/sec
0.018	0.014	140.9	55.87	55.67	-79.47	-79.47	-6.441	116.4	116.4
.054	.043	158.5	65.00	65.00	-66.98	-66.98	-5.428	143.6	143.6
.079	.063	163.7	69.83	69.83	-56.43	-56.43	-4.573	153.7	153.7
.104	.083	164.7	73.67	73.67	-46.31	-46.31	-3.753	158.0	158.0
.129	.103	166.6	76.83	76.83	-37.95	-37.95	-3.076	162.2	162.2
.154	.123	167.1	79.25	79.25	-31.17	-31.17	-2.526	164.2	164.2
.179	.143	169.3	81.67	81.67	-24.54	-24.54	-1.989	167.5	167.5
.229	.183	171.4	85.42	85.42	-13.70	-13.70	-1.110	170.8	170.8
.279	.223	170.9	88.00	88.00	-5.97	-5.97	-.484	170.8	170.8
.379	.303	170.6	91.25	91.25	3.72	3.72	.302	170.6	170.6
.479	.383	170.7	92.50	92.50	7.45	7.45	.604	170.6	170.6
.579	.463	169.3	93.00	93.00	8.86	8.86	.718	169.1	169.1
.679	.543	168.8	93.08	93.08	9.08	9.08	.736	168.6	168.6
.779	.623	167.4	92.58	92.58	7.54	7.54	.611	167.2	167.2
.879	.703	166.9	91.00	91.00	2.91	2.91	.236	166.9	166.9
.929	.743	168.6	89.50	89.50	-1.47	-1.47	-.119	168.5	168.5
.979	.783	166.6	87.50	87.50	-7.27	-7.27	-0.589	166.5	166.5
1.029	.823	164.9	85.08	85.08	-14.13	-14.13	-1.145	164.3	164.3
1.079	.863	163.1	81.67	81.67	-23.64	-23.64	-1.916	161.4	161.4
1.129	.903	160.7	77.25	77.25	-35.47	-35.47	-2.875	156.7	156.7
1.154	.923	156.6	73.92	73.92	-43.39	-43.39	-3.517	150.5	150.5
1.179	.943	155.1	70.25	70.25	-52.40	-52.40	-4.247	146.0	146.0
1.204	.963	149.3	65.33	65.33	-62.29	-62.29	-5.048	135.6	135.6
1.226	.981	138.8	60.17	60.17	-69.06	-69.06	-5.597	120.4	120.4

^aAverage radial velocities, $u_{av,om} = -12.34$ ft/sec, $u'_{av,i} = -12.42$ ft/sec, $u_{av,i} = -12.42$ ft/sec.

^bAverage tangential velocity; $v_{av,i} = 160.5$ ft/sec.

TABLE I. - Continued. VELOCITY COMPONENTS DATA

(f) Radial station, 3.5 inches. Temperature, 79.5° F; density, 0.104 pound mass per square foot; absolute pressure, 42.7 inches of mercury.

Axial coordinate		Velocity vector magnitude V, ft/sec	Velocity vector direction		Radial velocity component ^a			Tangential velocity component	
z, in.	$\bar{z} = z/L$		Observed θ' , deg	Corrected θ , deg	Observed u', ft/sec	Corrected u, ft/sec	Normalized u/u _{av, om}	Observed v', ft/sec	Corrected v, ft/sec
0.018	0.014	120.0	59.08	59.08	-61.65	-61.65	-5.881	102.9	102.9
.054	.043	137.4	68.17	68.17	-51.10	-51.10	-4.875	127.5	127.5
.079	.063	140.9	72.67	72.67	-41.96	-41.96	-4.003	134.5	134.5
.104	.083	143.7	76.00	76.00	-34.75	-34.75	-3.315	139.4	139.4
.129	.103	144.8	78.67	78.67	-28.45	-28.45	-2.714	141.9	141.9
.154	.123	144.8	80.92	80.92	-22.85	-22.85	-2.180	143.0	143.0
.179	.143	146.4	82.92	82.92	-18.05	-18.05	-1.722	145.3	145.3
.229	.183	147.5	85.75	85.75	-10.93	-10.93	-1.043	147.1	147.1
.279	.223	147.5	88.00	88.00	-5.15	-5.15	-.491	147.4	147.4
.379	.303	147.5	90.92	90.92	2.36	2.36	.225	147.5	147.5
.479	.383	147.5	92.33	92.33	6.00	6.00	.572	147.4	147.4
.579	.463	147.5	93.25	93.25	8.36	8.36	.798	147.3	147.3
.679	.543	147.5	93.25	93.25	8.36	8.36	.798	147.3	147.3
.779	.623	147.0	92.25	92.25	5.77	5.77	.550	146.8	146.8
.879	.703	147.0	90.25	90.25	.64	.64	.061	147.0	147.0
.929	.743	145.3	88.83	88.83	-2.96	-2.96	-.282	145.3	145.3
.979	.783	144.8	86.83	86.83	-8.00	-8.00	-.763	144.5	144.5
1.029	.823	144.2	84.83	84.83	-12.99	-12.99	-1.239	143.6	143.6
1.079	.863	143.1	81.75	81.75	-20.53	-20.53	-1.959	141.6	141.6
1.129	.903	139.7	77.67	77.67	-29.84	-29.84	-2.847	136.5	136.5
1.154	.923	137.8	74.75	74.75	-36.23	-36.23	-3.456	132.9	132.9
1.179	.943	134.6	71.25	71.25	-43.26	-43.26	-4.127	127.4	127.4
1.204	.963	129.4	67.00	67.00	-50.55	-50.55	-4.822	119.1	119.1
1.227	.982	118.4	61.92	61.92	-55.73	-55.73	-5.316	104.4	104.4

^aAverage radial velocities, $u_{av, om} = -10.5$ ft/sec, $u'_{av, i} = -10.0$ ft/sec, $u_{av, i} = -10.0$ ft/sec.

^bAverage tangential velocity; $v_{av, i} = 140.0$ ft/sec.

TABLE I. - Continued. VELOCITY COMPONENTS DATA

(g) Radial station, 4.5 inches. Temperature, 75.5° F; density, 0.106 pound mass per cubic foot; absolute pressure, 43.0 inches of mercury.

Axial coordinate		Velocity vector magnitude V, ft/sec	Velocity vector direction		Radial velocity component ^a			Tangential velocity component	
z, in.	$\bar{z} = z/L$		Observed θ' , deg	Corrected θ , deg	Observed u', ft/sec	Corrected u, ft/sec	Normalized u/u _{av,om}	Observed v', ft/sec	Corrected v, ft/sec
0.018	0.014	88.4	64.83	64.23	-37.60	-38.44	-4.786	80.0	79.6
.054	.043	102.0	72.25	71.65	-31.09	-32.11	-3.998	97.1	96.8
.079	.063	104.3	75.25	74.65	-26.55	-27.61	-3.437	100.9	100.6
.104	.083	105.8	77.67	77.07	-22.60	-23.68	-2.948	103.3	103.1
.129	.103	107.0	79.67	79.07	-19.19	-20.29	-2.526	105.2	105.0
.154	.123	108.3	81.67	81.07	-15.69	-16.82	-2.094	107.2	107.0
.179	.143	109.9	82.92	82.32	-13.55	-14.69	-1.829	109.0	108.9
.229	.183	111.6	85.42	84.82	-8.92	-10.08	-1.255	111.2	111.1
.279	.223	113.4	87.42	86.82	-5.11	-6.30	-0.784	113.3	113.2
.379	.303	114.8	90.08	89.48	.17	-1.04	-.130	114.8	114.8
.479	.383	115.3	91.33	90.73	2.68	1.48	.184	115.3	115.3
.579	.463	116.2	91.92	91.32	3.89	2.67	.332	116.1	116.1
.679	.543	116.8	91.58	90.98	3.23	2.00	.249	116.8	116.8
.779	.623	115.8	90.58	89.98	1.18	-.03	-.004	115.7	115.8
.879	.703	114.4	89.17	88.57	-1.66	-2.86	-.356	114.4	114.3
.929	.743	112.3	88.08	87.58	-3.76	-4.93	-.614	112.2	112.2
.979	.783	111.6	87.08	86.48	-5.68	-6.85	-.853	111.4	111.4
1.029	.823	110.2	85.92	85.32	-7.84	-8.99	-1.119	109.9	109.8
1.079	.863	109.2	84.42	83.82	-10.62	-11.76	-1.464	108.6	108.5
1.129	.903	107.0	81.83	81.23	-15.20	-16.30	-2.029	105.9	105.7
1.154	.923	104.3	79.58	78.98	-18.26	-19.93	-2.481	102.6	102.4
1.179	.943	100.4	76.42	75.82	-23.59	-24.61	-3.064	97.6	97.4
1.204	.963	92.6	72.00	71.40	-28.61	-29.53	-3.676	88.1	87.8
1.216	.973	86.6	69.25	68.65	-30.69	-31.53	-3.925	81.0	80.7

^aAverage radial velocities, u_{av,om} = -8.03 ft/sec, u'_{av,i} = -6.85 ft/sec, u_{av,i} = -7.98 ft/sec.

^bAverage tangential velocity, v_{av,i} = 107.7 ft/sec.

TABLE II. - DIMENSIONAL AND NORMALIZED MEASURED STATIC-PRESSURE DISTRIBUTIONS

Radial coordinate, in.		Pressure differences ^a													
r	$\bar{r} = \frac{r}{r_0}$	$p(1.0) - p(r_0)$	$\frac{p(1.0) - p(r_0)}{\rho v_0^2}$	$p(1.5) - p(r_0)$	$\frac{p(1.5) - p(r_0)}{\rho v_0^2}$	$p(2.0) - p(r_0)$	$\frac{p(2.0) - p(r_0)}{\rho v_0^2}$	$p(2.5) - p(r_0)$	$\frac{p(2.5) - p(r_0)}{\rho v_0^2}$	$p(3.0) - p(r_0)$	$\frac{p(3.0) - p(r_0)}{\rho v_0^2}$	$p(3.5) - p(r_0)$	$\frac{p(3.5) - p(r_0)}{\rho v_0^2}$	$p(4.5) - p(r_0)$	$\frac{p(4.5) - p(r_0)}{\rho v_0^2}$
1.0	.171	-63.30	-11.97	-59.65	-11.28	-58.85	-11.13	-59.40	-11.23	-59.97	-11.34	-59.07	-11.17	-59.07	-11.17
1.5	.256	-30.20	-5.71	-31.30	-5.92	-30.75	-5.82	-30.75	-5.82	-30.92	-5.85	-30.47	-5.76	-30.52	-5.77
2.0	.341	-16.50	-3.12	-16.85	-3.19	-16.60	-3.14	-16.60	-3.14	-16.67	-3.15	-16.42	-3.11	-16.52	-3.12
2.5	.427	-10.6	-2.00	-10.3	-1.95	-10.10	-1.91	-10.20	-1.93	-10.25	-1.94	-9.67	-1.83	-10.12	-1.91
3.0	.512	-7.05	-1.33	-6.85	-1.30	-6.70	-1.27	-6.75	-1.28	-6.82	-1.29	-6.72	-1.27	-6.72	-1.27
3.5	.597	-4.50	-.85	-4.60	-.87	-4.50	-.85	-4.50	-.85	-4.47	-.85	-4.37	-.83	-4.52	-.85
4.5	.768	-1.65	-.312	-1.6	-.30	-1.55	-.293	-1.60	-.30	-1.52	-.29	-1.55	-.29	-1.52	-.29
Radial station of probe	r	1.0		1.5		2.0		2.5		3.0		3.5		4.5	
	\bar{r}	.171		.256		.341		.427		.512		.597		.768	

^a $p(r) - p(r_0)$ in inches of water
 $\frac{p(r) - p(r_0)}{\rho v_0^2}$ dimensionless

3/1 8/85
62 ✓

"The aeronautical and space activities of the United States shall be conducted so as to contribute . . . to the expansion of human knowledge of phenomena in the atmosphere and space. The Administration shall provide for the widest practicable and appropriate dissemination of information concerning its activities and the results thereof."

—NATIONAL AERONAUTICS AND SPACE ACT OF 1958

NASA SCIENTIFIC AND TECHNICAL PUBLICATIONS

TECHNICAL REPORTS: Scientific and technical information considered important, complete, and a lasting contribution to existing knowledge.

TECHNICAL NOTES: Information less broad in scope but nevertheless of importance as a contribution to existing knowledge.

TECHNICAL MEMORANDUMS: Information receiving limited distribution because of preliminary data, security classification, or other reasons.

CONTRACTOR REPORTS: Technical information generated in connection with a NASA contract or grant and released under NASA auspices.

TECHNICAL TRANSLATIONS: Information published in a foreign language considered to merit NASA distribution in English.

TECHNICAL REPRINTS: Information derived from NASA activities and initially published in the form of journal articles.

SPECIAL PUBLICATIONS: Information derived from or of value to NASA activities but not necessarily reporting the results of individual NASA-programmed scientific efforts. Publications include conference proceedings, monographs, data compilations, handbooks, sourcebooks, and special bibliographies.

Details on the availability of these publications may be obtained from:

SCIENTIFIC AND TECHNICAL INFORMATION DIVISION
NATIONAL AERONAUTICS AND SPACE ADMINISTRATION

Washington, D.C. 20546